Non-destructive tests for railway evaluation: Detection of fouling and joint interpretation of GPR data and track geometric parameters

Mercedes Solla[1] & Simona Fontul[2]

[1] Defense University Center, Spanish Naval Academy, Marín, Spain
MERCHISOLLA@CUD.UVIGO.ES

[2] National Laboratory For Civil Engineering (LNEC), Lisbon, Portugal
SIMONA@LNEC.PT

ABSTRACT

This paper deals with railway assessment by using Ground Penetrating Radar, eventually combined with Falling Weight Deflectometer and Light Falling Weight Deflectometer. All measurements were performed during a Short-Term Scientific Mission (STSM) funded by the COST (European Cooperation in Science and Technology) Action TU1208 "Civil engineering applications of Ground Penetrating Radar." In particular, the tasks addressed were: 1. Detection of track defects at infrastructure level (voids and cracking); 2. Measurement of layer thickness; and, 3. Evaluation of the fouling level of ballast.

KEYWORDS: Ground Penetrating Radar; Railways; Detection of track defects; Measurement of layer thickness; Fouling evaluation; Falling Weight Deflectometer.

1. INTRODUCTION

A Short-Term Scientific-Mission (STMS) entitled "Non-destructive tests for railway evaluation: detection of fouling and joint interpretation of GPR data and track geometric parameters" was funded in 2015 by COST (European Cooperation in Science and Technology), in the framework of the COST Action TU1208 "Civil engineering applications of Ground Penetrating Radar" activities. Mercedes Solla visited Simona Fontul in Lisbon, Portugal, from June 1st to June 30th, 2017, and they jointly carried out a series of experiments concerned with the non-destructive assessment of railways. The objective of this paper is to present the results obtained during the STSM.

Railways, as all infrastructures, have to behave properly during their life cycle. A regular maintenance policy has to be established, to guarantee high safety standards [1]. At the same time, costs and traffic interruptions have to be limited. Nowadays, track monitoring mainly consists in measuring parameters related to the track layout and rail wearing. During maintenance operations, some track components are replaced while others can remain the same, such as the substructure [2, 3]. The customary monitoring procedure does not detect the real causes of rail deficiency, which may be due to the presence of ballast pockets, fouled ballast, poor drainage, subgrade settlements or transitions problems [4-6]. A more thorough analysis of the conditions of both the railway platform and substructure is crucial to reduce maintenance costs and increase operational safety levels.

Non-destructive testing techniques can be effectively employed for railway assessment. The main purpose of the STSM was to study how Ground Penetrating Radar (GPR) can be used to inspect the infra- and super-structure of railways. In particular, the tasks addressed were: 1. Detection of track defects at infrastructure level (voids and cracking); 2. Measurement of layer thickness; and, 3. Evaluation of the fouling level of ballast.

Two different GPR systems were used and compared, in terms of their capability to detect defects in the subgrade (at platform level) and estimate the dielectric permittivity of concrete asphalt for sub-ballast. In particular, the available equipment included: a ground-coupled GPR manufactured by MALÅ (brought to Lisbon from the University of Vigo, Spain) and an air-coupled system manufactured by GSSI (available at the National Laboratory For Civil Engineering, in Lisbon). The MALÅ system was a ProEx control unit equipped with 1-GHz and 2.3-GHz antennas. The GSSI system was a SIR-20 control unit equipped with 1-GHz and 1.8-GHz antennas. The accuracy of different inspection procedures was evaluated, to determine the best way to proceed for assessing railways with GPR.

2. MATERIALS

2.1 TASK 1: DETECTION OF TRACK DEFECTS AT INFRASTRUCTURE LEVEL

The experimental activities were carried out in the test site shown in Figure 1. Metal plates located in the subgrade were very useful for data

interpretation and for the calibration of the air-coupled antenna (see the schemes reported in Figure 2). The soil employed to realise the road base is classified by the Unified Soil Classification System as clay of low plasticity, or lean clay. In the gradation test, 66% of such material passes the No. 200 sieve. The Atterberg limits are: plastic limit 19.9% and liquid limit 46.5%, which lead to a plasticity index of 26.6.

FIG. 1 – Photos showing the test site at LNEC and GPR data acquisition with ground- and air-coupled antennas.
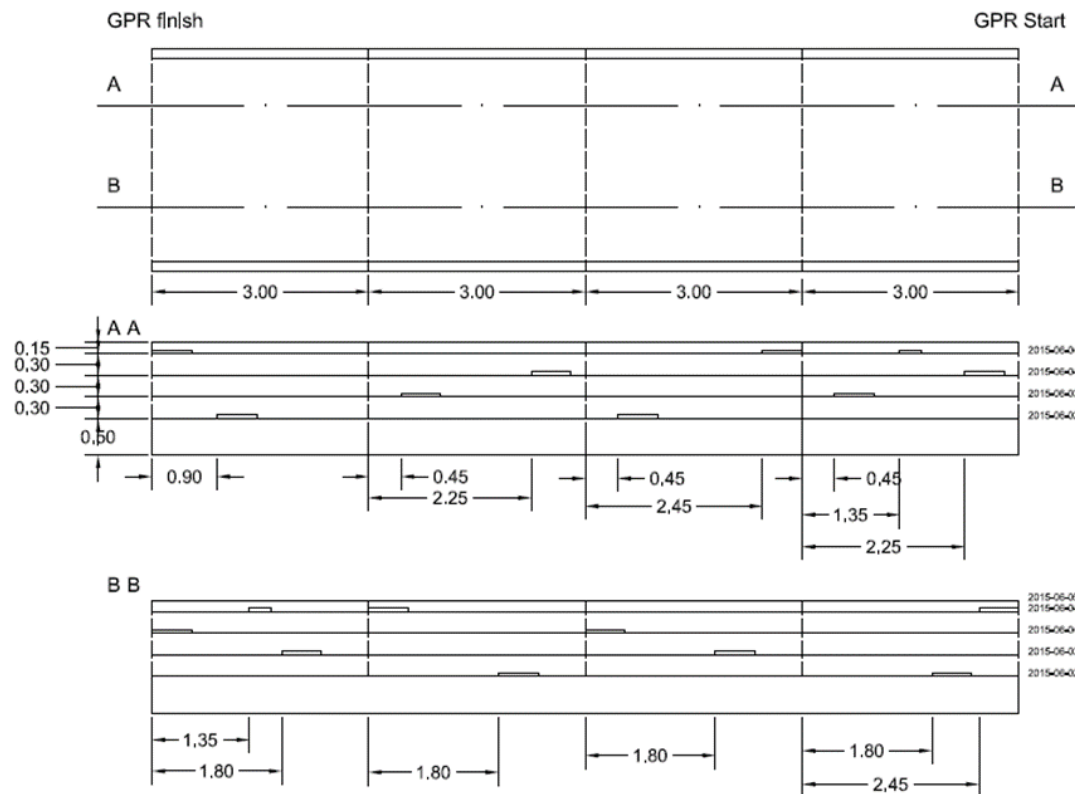
FIG. 2 – Map of the inspected area and configuration of metal plates disposed in the subgrade.

2.2 TASK 2: MEASUREMENT OF LAYER THICKNESS

The experimental activities were carried out in the test site shown in Figure 3. Three different railway substructures are present in this test pit structure. They were suitably modified to serve the purposes of this study. In particular, the test site is divided into two sections: one of them has a square area of 4.0 m × 4.0 m and a depth of 2.80 m, with concrete floor and walls (concrete pit section); the other section is rectangular with a 4.0 m × 6.0 m area and a 2.60-m depth. In order to ensure a homogeneous subgrade, the existing materials were excavated and replaced with new ones. As shown in Figure 4, three different infrastructure solutions were implemented (Cells 2 to 4), where various non-conventional railway substructures using asphalt sub-ballast were constructed, instead of conventional structures using granular sub-ballast.
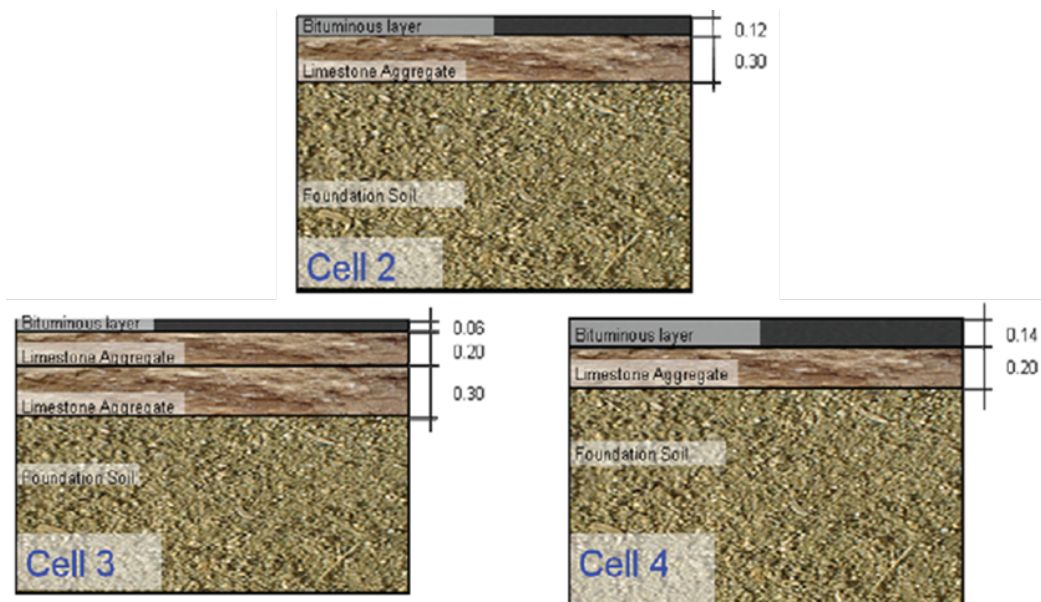
FIG. 3 – Test site at LNEC, for task 2.

FIG. 4 – Test-site sections of the three Cells.

2.3   TASK 3: EVALUATION OF THE FOULING LEVEL OF BALLAST.

Different conditions of ballast were simulated to study how they affect the measured GPR signal. In particular, data gathered on new ballast

were compared to data gathered on old or used ballast. Moreover, the influence of fouling conditions as well as of water content was studied.

Firstly, two specimens (Boxes 1 and 2) were built and the dielectric constant was estimated for both the new and used (old) ballast (see Figure 5). The material was compacted with a VIBRO-VERKEN system by applying a weigh of 57 Kg with 2850 pulses/min for a total of 2 min. To calibrate the dielectric constants of ballast, each box has two points with controlled height (see Table 1). Moreover, aluminium foil was introduced at the bottom of the boxes to reflect the signal in order to facilitate the thickness measurement.

FIG. 5 – Boxes containing new (left) and used (right) ballast.

Then, two specimens (Boxes 3 and 4) were built to study the influence of fouling and water content on the dielectric constant. New ballast was included in Box 3 and used ballast in Box 4. To simulate fouling, a layer of soil with high level of clays was merged every two consecutive layers of ballast (see Figure 6).

The specimen built to simulate 7.5% of fouling (Box 3) was composed of: 1 layer of ballast + 1.5 kg of soil + 1 layer of ballast + 1.5 kg of soil + 1 layer of ballast + 1.5 kg of soil + 1 layer of ballast + 1.5 kg soil + 1 layer of ballast; the average total height of the specimen resulted equal to about 18 cm.

The specimen built to simulate 15% of fouling (Box 4) was composed of: 1 layer of ballast + 3 kg of soil + 1 layer of ballast + 3 kg of soil + 1 layer of ballast + 3 kg of soil + 1 layer of ballast + 3 kg of soil + 1 layer of ballast. The average total height of the specimen resulted equal to about 18 cm.

These two specimens were compacted, same as Boxes 1 and 2, and their final configuration is described in Table 1.

TABLE 1 – MAIN PROPERTIES OF THE SPECIMENS:
TYPE OF BALLAST, FOULING AND WATER CONTENT.

Specimen	Characteristics	Control points		Fouling	Water content
		1	2		
Box 1	New ballast	17 cm	18 cm	0%	----
Box 2	Used ballast	17 cm	18 cm	0%	----
Box 3	New ballast	17 cm	18 cm	7.5%	5.5%
					10%
					14%
Box 4	Used ballast	17 cm	17 cm	15%	5.5%
					10%
					14%

FIG. 6 – Distribution of soil between two consecutive layers of ballast.

The initial water content of the soil was measured. A sample of soil was dried for one day at 104º, which resulted in 5.5% of water content. The wet and dried weights of the sample were 245.38 g and 231.76 g, respectively. Different water contents were then considered: as described in Table 2, different quantities of water were scattered in the Boxes 3 and 4 (see Figure 7) to reach water content levels of 10% and 14%. The purpose of such tests was to simultaneously study the effect of fouling and water content. Better results can be obtained by using larger boxes.

TABLE 2 – PROPERTIES OF SPECIMENS USED TO SIMULTANEOUSLY ANALYSE FOULING AND WATER CONTENT EFFECTS.

Specimen	Characteristics	Fouling	Water content	Water [kg]
Box 1	New ballast	0%	----	----
Box 2	Used ballast	0%	----	----
Box 3	New ballast	7.5%	5.5%	----
			10%	0.54
			14%	+0.48
Box 4	Used ballast	15%	5.5%	----
			10%	0.27
			14%	+0.24

FIG. 7 – Introduction of water in the specimens.

3. METHODS

3.1 TASK 1: DETECTION OF TRACK DEFECTS AT INFRASTRUCTURE LEVEL

When using the ground-coupled system, data were recorded with a trace-interval of 0.01 s. Marks were taken when collecting data, to subsequently correlate them with those measured by the air-coupled system.

When using the air-coupled system, data were recorded with a trace-interval of 1.0 cm.

Additionally, a Falling Weight Deflectometer (FWD) (see Figure 8 – upper panel) was used to evaluate the bearing capacity of the subgrade. The thicknesses obtained from GPR data were combined with deflections measures with FWD, to produce the structural models of the subgrade layers. For a given thickness, the deflection values is higher if the elastic moduli of the subgrade is lower, which could be interpreted as an anomalous zone and can be due to cracking, interlayer debonding or construction failures.

Light Falling Weight Deflectometer (LFWD) measures were also performed (see Figure 8 – lower panel), to add more information and further validate the interpretation of the damaged areas identified by GPR and FWD.

Finally, in order to corroborate the joint interpretation of GPR-FWD-LFWD data, drill cores were extracted in the detected damaged areas (see Figure 9).

3.2 TASK 2: MEASUREMENT OF LAYER THICKNESS

The purpose of the tests was to analyse the accuracy of the GPR systems used in this STSM for thickness measurement. Different GPR systems and antenna configuration were employed (see Figure 10). Different methodologies were considered to gather data and characterize the asphalt (first bituminous layer in Figure 4).

The ground-coupled system was equipped with antennas having central frequencies of 1 GHz and 2.3 GHz. During data acquisition, the antennas were moved along the surface line and data were recorded in both static and dynamic modes.

The air-coupled system was equipped with antennas having central frequencies of 1 GHz and 1.8 GHz. The antennas were at about 45-50 cm from the inspected surface. Also in this case, data were acquired in both static and dynamic modes.

Table 3 resumes the data acquisition settings.

FIG. 8 – Upper panel: Portable FWD. Lower panel: LFWD.

FIG. 9 – Extraction of drill cores.

TABLE 3 – CONFIGURATIONS USED FOR DATA ACQUISITION.

Antennas		Ground-coupled		Air-coupled	
Frequency [GHz]		**1.0**	**2.3**	**1.0**	**1.8**
Time windows [ns]		43	14	20	12
Samples/scan		500	292	1024	1024
Trace-interval	Dynamic mode [cm]	0.02	0.02	0.02	0.02
	Static mode [s]	0.02	0.02	---	---
	Static mode [Scans/s]	---	---	60	60

The static data were used to calibrate the velocity of propagation of the GPR signal in asphalt; the dynamic data allowed for a comparison between methodologies. For each system, two different GPR lines were acquired by distance in all the cells (see Figure 4). The static data were gathered at two control points on each profile line. After surveying, drill cores were extracted through the bituminous layer at these control points to proceed with calibration (see Table 4).

Two different methodologies were employed to calibrate the velocity of propagation and to measure thicknesses, as described in the following.

FIG. 10 – Data acquisition. Upper panel: ground-coupled system with 1.0 GHz (right) and 2.3 GHz (left) antennas. Lower panel: air-coupled system with 1.0 GHz and 1.8 GHz antennas.

Coring – for both ground-and air-coupled antennas.

Knowing the thickness of the layers (d) from coring and the travel time difference (twt) to and from the target, the velocity of propagation (v) can be derived from Equation (1). Next, the relative dielectric constant (ε) can be obtained from Equation (2).

$$d = v\frac{twt}{2} \tag{1}$$

$$\varepsilon = \left(\frac{c}{v}\right)^2 \tag{2}$$

where c is the free-space velocity (0.3 m/ns).

TABLE 4 – THICKNESSES OF THE BITUMINOUS LAYER (AT THE CONTROL POINTS) OBTAINED FROM CORING

Cell	Line	Control point	Thickness [m]
2	3	3.1	0.112
		3.2	0.115
	4	4.1	0.116
		4.2	0.115
3	5	5.1	0.064
		5.2	0.055
	6	6.1	0.055
		6.2	0.053
4	7	7.1	0.133
		7.2	0.134
	8	8.1	0.135
		8.2	0.128

Metal plate – for air-coupled antennas, only.

By knowing the amplitudes of the reflected pulses (with and without the metal plate) and their arrival times, it is possible to estimate the dielectric constant and thickness of a layer.

The first step in the process is determining the dielectric constant. The amplitude of the incident GPR signal and the amplitude of the layer return are necessary for the calculations. In particular, the amplitude of the incident GPR signal can be determined by collecting data over a large flat metal plate, placed on the surface to be inspected, and by measuring the amplitude of the reflected signal. Because metal is a good conductor, it can be considered as a perfect reflector: hence, the amplitude of the reflected signal can be considered equal to the amplitude of the incident signal. The relative dielectric constant of the first layer of the inspected structure is given by:

$$\varepsilon_a = \left[\frac{1+\frac{A_1}{A_m}}{1-\frac{A_1}{A_m}}\right]^2 \tag{3}$$

where A_1 is the amplitude of the reflection from the surface, without metal plate, and A_m is the amplitude of the reflection from a large metal plate.

Next, the amplitude profiles are transformed into layer thickness profiles as follows:

$$d = \frac{c \ twt}{\sqrt{\varepsilon}} \tag{4}$$

where the distance travelled by the radar-wave (d) is equal to the thickness of the layer, c is the speed of light, twt is the two-way travel-time distance between two different reflectors (layers), and ε is the relative dielectric constant obtained from Equation (3).

3.3 TASK 3: EVALUATION OF THE FOULING LEVEL OF BALLAST.

Static measurements were carried out at the control points. Data were gathered by using both the ground- and air-coupled systems, with a trace-interval of 0.01 s. The data acquisition with the ground-coupled system was conducted with the antennas in contact with the ballast, without elevation; the air-coupled antennas, instead, were at about 40 cm from the inspected surface.

4. RESULTS

4.1 TASK 1: DETECTION OF TRACK DEFECTS AT INFRASTRUCTURE LEVEL

In the following radargrams, red rectangles indicate the metal plates and yellow circles are the possible damaged areas.

Location 1: through the middle of the test site (see Figure 2)

The comparison of the 1.0 GHz data obtained with both ground- and air-coupled antennas, presented in Figures 11 and 12, respectively, demonstrates that the ground-coupled system is capable to provide a better resolution, which allows for a better definition of the anomalous zones. In Figure 13, 1.8 GHz data obtained with the air-coupled system are reported. The 2.3-GHz data obtained with the ground-coupled

system and presented in Figure 14(a) have an even better resolution than the 1.0-GHz data of Figure 11.

FWD measurements were carried out in the same positions where the GPR profiles were recorded, in the middle of the experimental area.
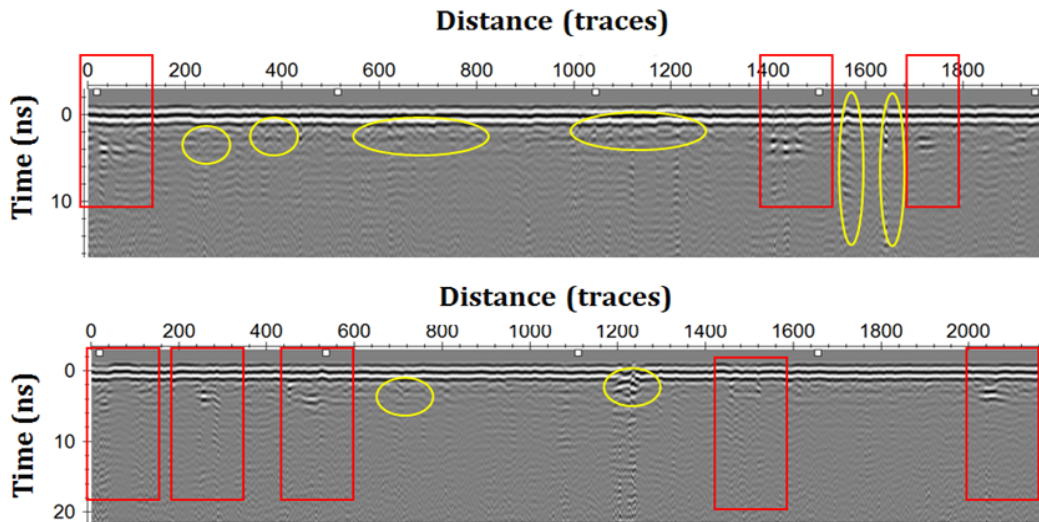

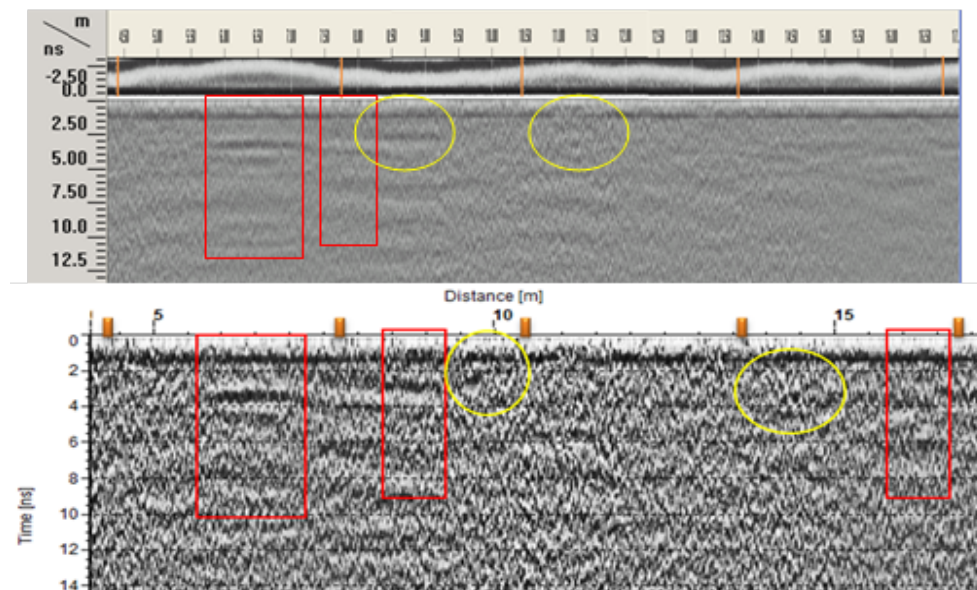**FIG. 11 –** 1.0 GHz data obtained with the ground-coupled system.

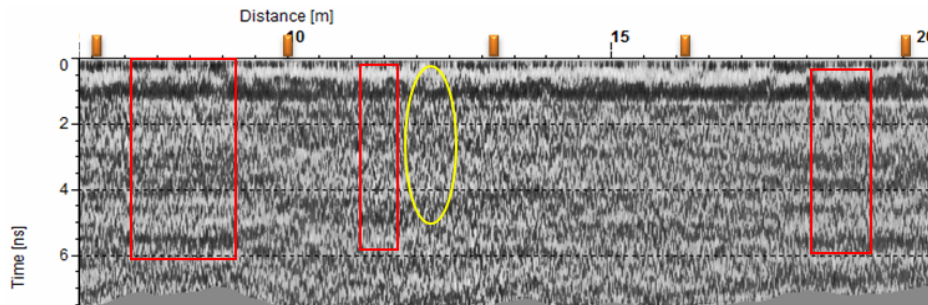**FIG. 12 –** 1.0 GHz data obtained with the air-coupled system.

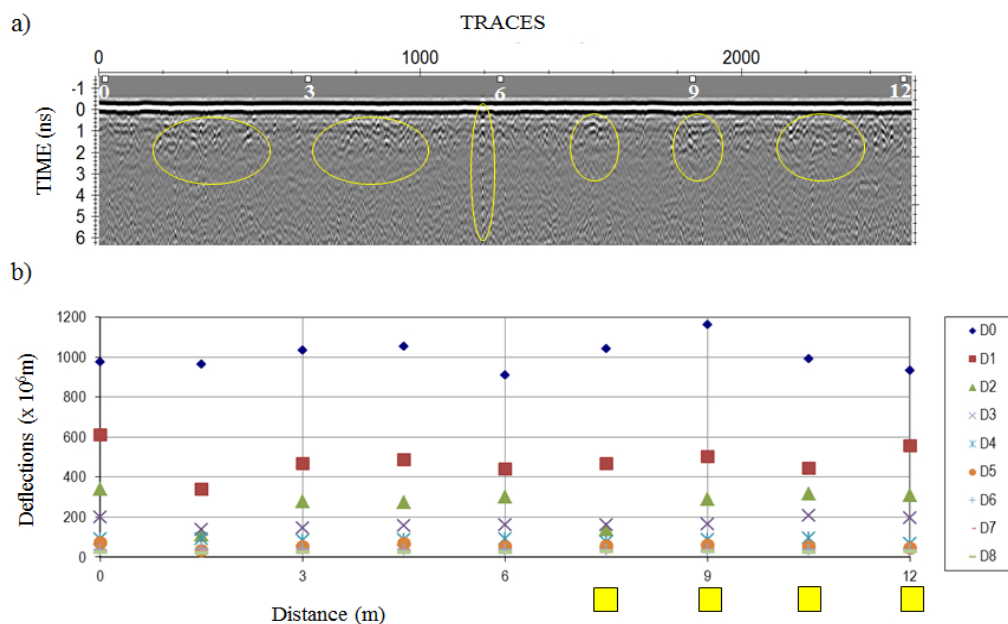**FIG. 13 –** 1.8 GHz data obtained with the air-coupled system.

FIG. 14 – (a) 2.3 GHz data obtained with the ground-coupled system, and (b) deflections produced by FWD (yellow squares indicate where drill cores were extracted).

In Figure 14(b), it can be observed that the places representing more noise correspond to FWD results with anomalous deflections. For example, at positions 1.5 m and 7.5 m, there is a difference in deflection trend D3 higher than D2. In almost all the points, see position 9.0 m, there is a small difference between D0 and D1. The anomalies can be due to cracking on the soil top layer (9.0 m) or even in the layer beneath (1.5 m and 7.5 m), or to debonding. The only two positions that present better continuity of the deflections are 0.0 and 12.0 m. This means that

the load transmission is better and so the continuity of the layer is better (or else there is a lower cracking).

By comparing FWD data with 2.3-GHz data in Figure 15(a), it was corroborated the good agreement between the methods when identifying both anomalous deflections and reflections. The anomaly identified at 7.5 m was also detected in the 1.0-GHz data produced by the air-coupled system (Figure 13). This interpretation is more detailed in the graphics reported in Figure 15.
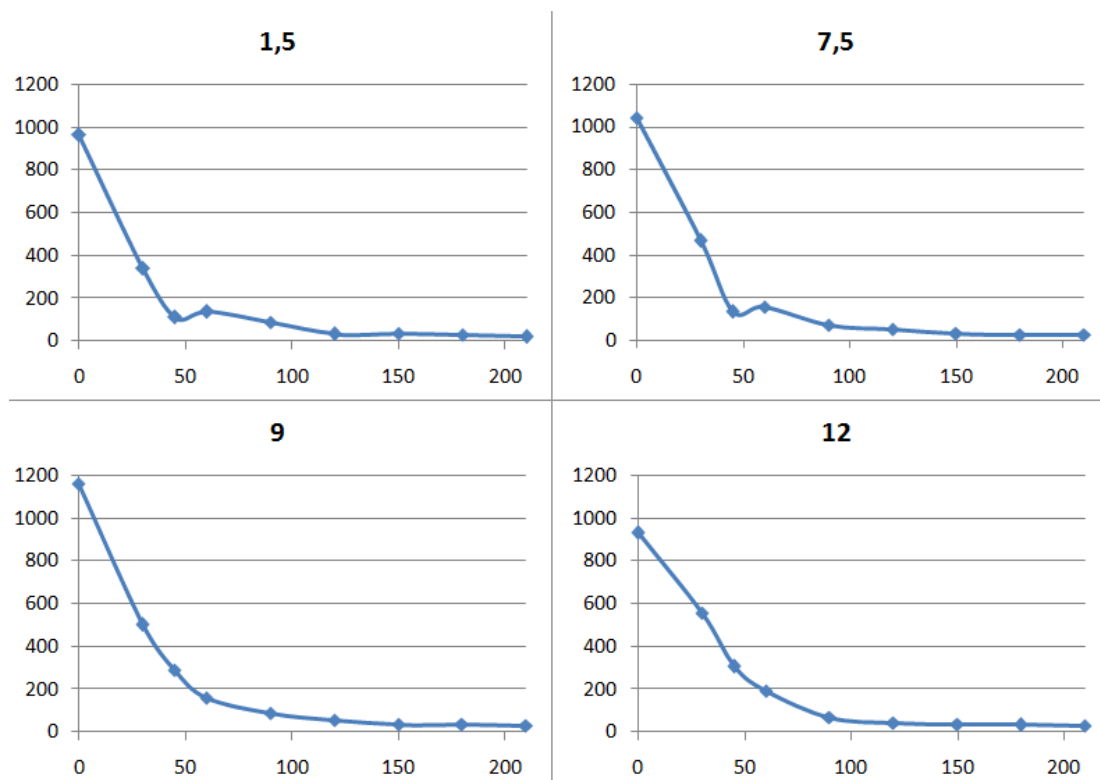
FIG. 15 – Graphics from FWD data, showing the most affected areas.

LFWD measures were performed to further validate the interpretation of the damaged areas achieved from GPR and FWD methods. Figure 16 presents the LFWD data obtained through the middle of the test site, which corroborate the existence of anomalies or damaged zones at 1.5 m, 7.5 m and 9.0 m - 10.5 m positions.

Finally, coring was performed in the areas showing the most apparent anomalies (7.5 m, 9.0 m and 10.5 m). In addition, a drill core was

extracted in a position where no anomalies were detected (12.0 m). The positions of such cores are illustrated by yellow squares in Figure 14(b). Figure 17 shows the drill cores extracted. The core extracted at 7.5 m presents severe cracking in the subgrade, while the one extracted at 9.0 m shows defects between layers (delamination).
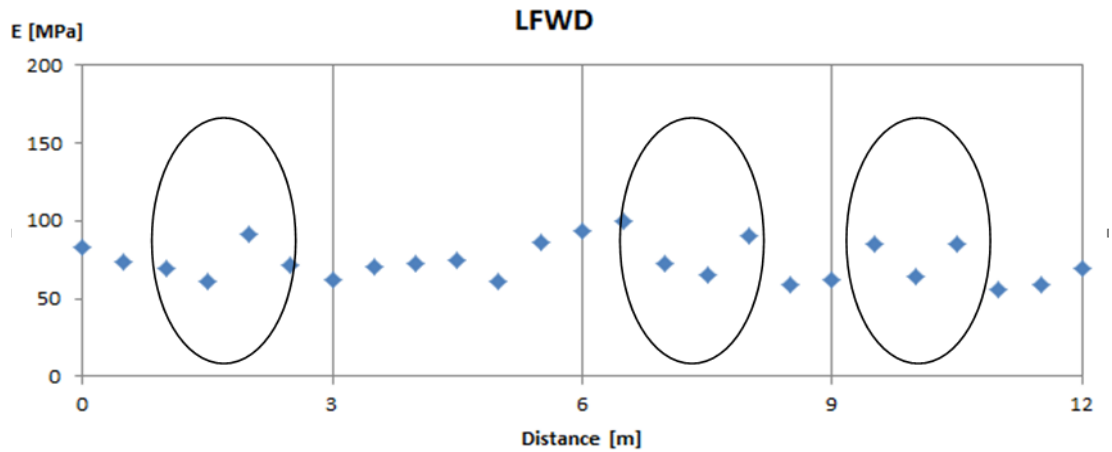

FIG. 16 – Deflections obtained from LFWD.
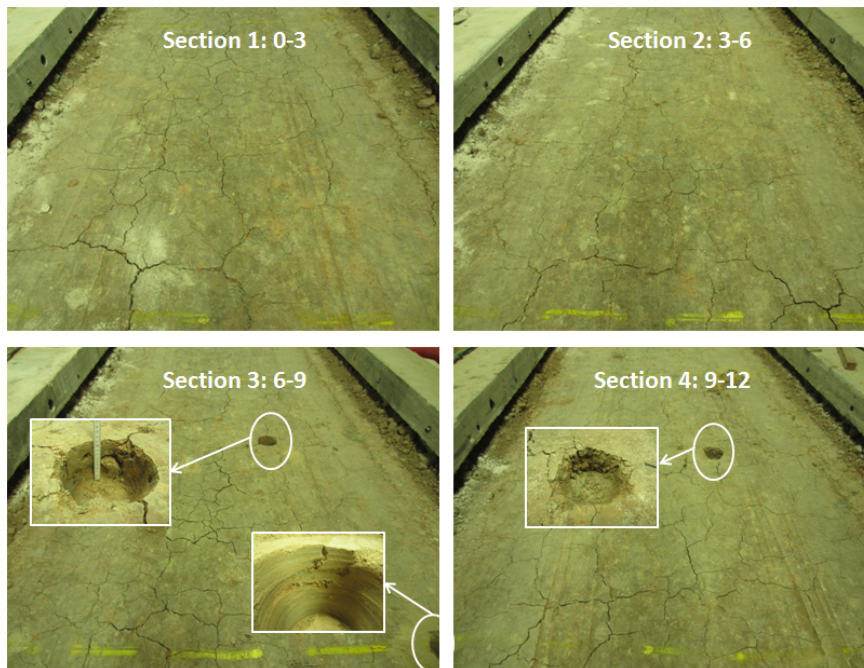
FIG. 17 – Drill cores extracted at positions 7.5 m, 9.0 m and 10.5 m shown in Figure 14.

FIG. 18 – Drill core extracted at 12.0 m, where no anomalies were detected.

Location 2: through the right side of the test site (B in Figure 2)

The GPR results that we obtained are presented in Figures 19-22.

Location 3: through left side of the test site (A in Figure 2)

A selection of GPR results is presented in Figures 23 and 24.

Through this series of experiments, it was demonstrated that ground-coupled systems present clear advantages compared to air-coupled systems: they provide deeper signal penetration and better vertical resolution, thus allowing to detect fine details, such as cracking.

FIG. 19 – 1.0 GHz data obtained with the ground-coupled system.

FIG. 20 – 1.0 GHz data obtained with the air-coupled system.

FIG. 21 – 1.8 GHz data obtained with the air-coupled system.
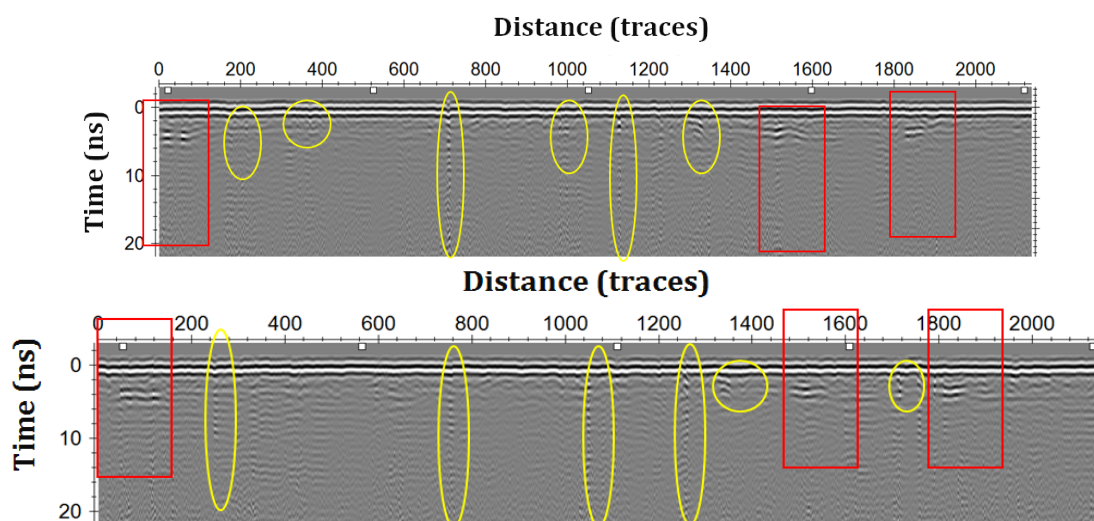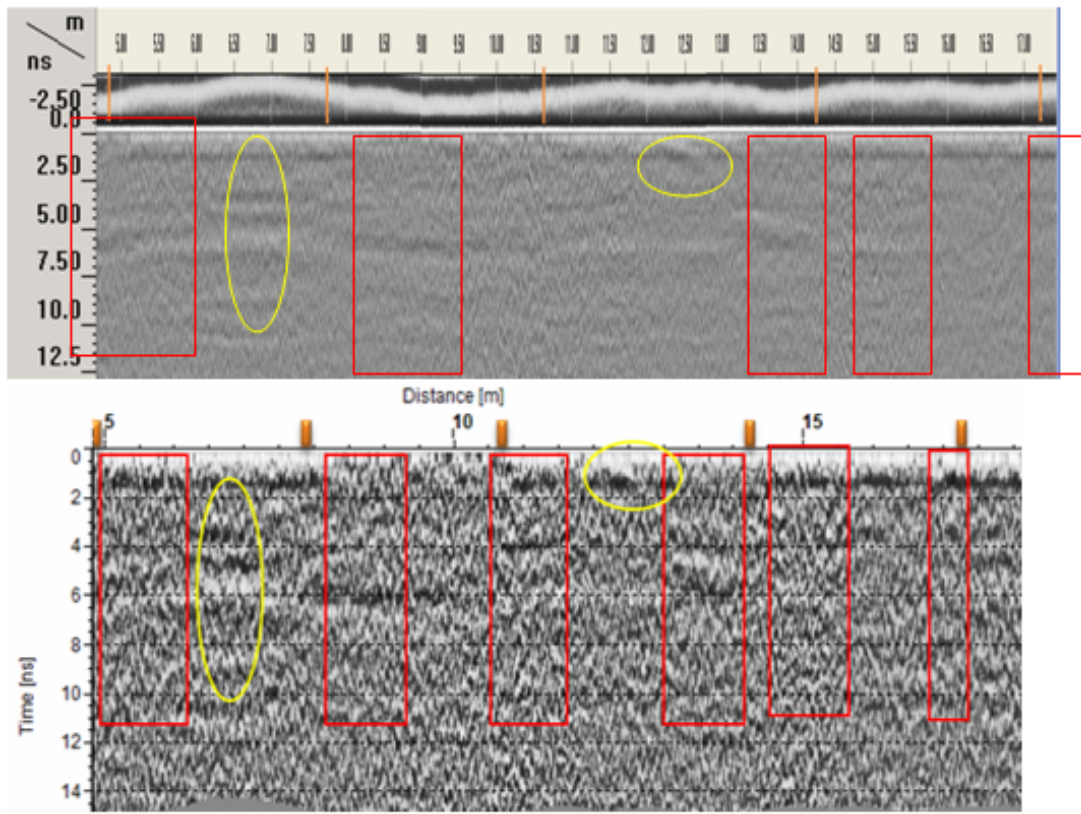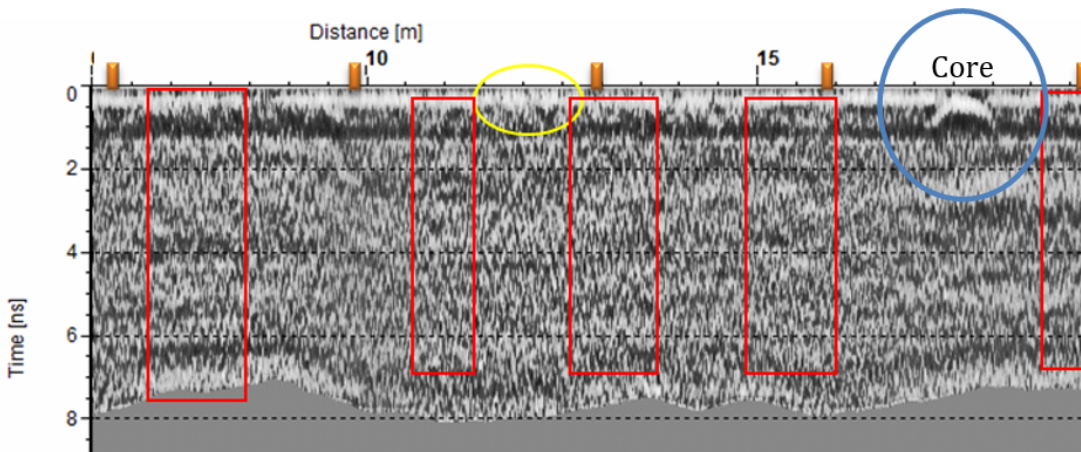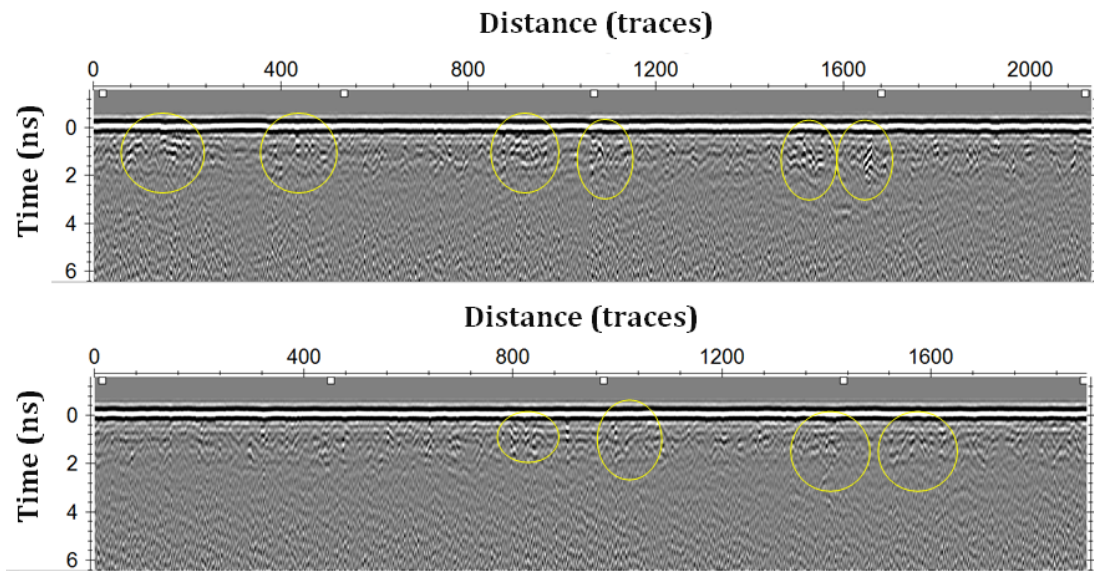
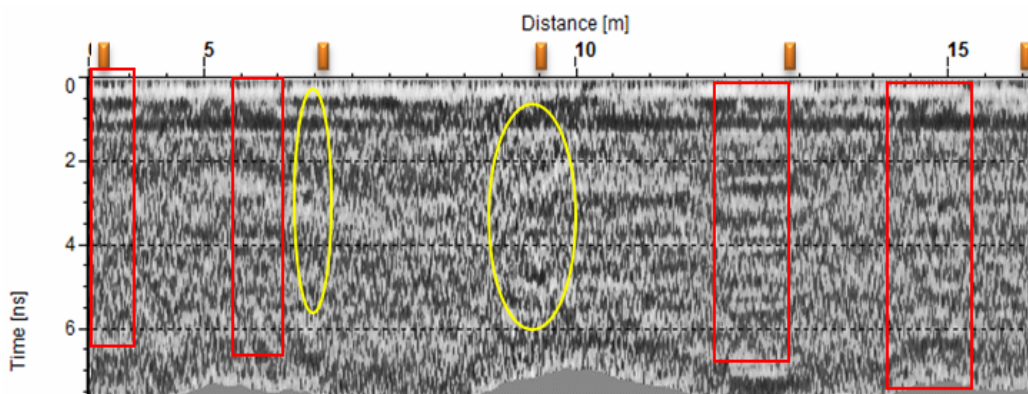**FIG. 22 –** 2.3 GHz data obtained with the ground-coupled system.

FIG. 23 – 1.8 GHz data obtained with the air-coupled system.
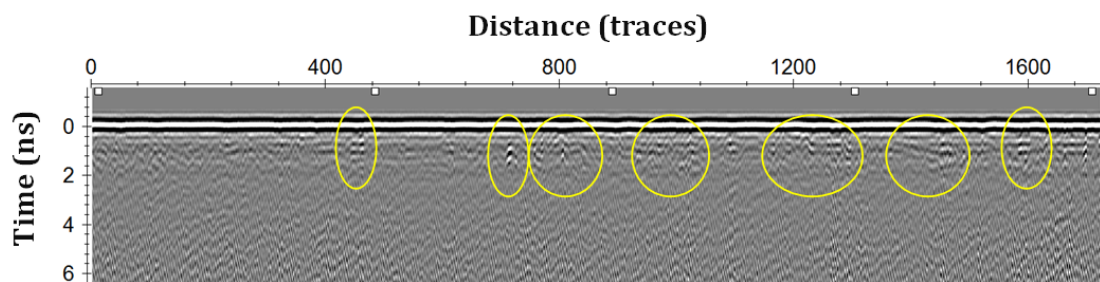

FIG. 24 – 2.3 GHz data obtained with the ground-coupled system.

4.2 TASK 2: MEASUREMENT OF LAYER THICKNESS

Bituminous thicknesses obtained by using the coring method

Tables 5 and6 show the dielectric constants and velocities obtained from the coring method for the first bituminous layer in Figure 4. For both ground- and air-coupled systems, these values were obtained from Equations (1) and (2) and by using the static data acquired at each control point of the three different cells.

Table 5 describes the dielectric constants and velocities of propagation obtained for the ground-coupled system (frequencies of 1.0 GHz and 2.3 GHz). The velocities obtained range from 0.121 m/ns to 0.137 m/ns, resulting in average values of 0.125 m/ns, 0.130 m/ns and 0.133 m/ns for Cells 2, 3 and 4, respectively.

Table 6 presents values obtained with the air-coupled antennas (frequencies of 1.0 GHz and 1.8 GHz). For the GSSI system, the velocities obtained range from 0.112 m/ns to 0.130 m/ns and average velocity values for Cells 2, 3 and 4 of 0.117 m/ns, 0.124 m/ns and 0.12 m/ns, respectively.

By comparing the dielectric constants obtained from both systems, it can be observed that the ground-coupled system provides lower values than the air-coupled system.

Knowing the velocity of propagation of the GPR signal in asphalt, the time-distance (ns) profiles obtained from dynamic data acquisition can be converted into thicknesses profiles (m) by using Equation (1).

Bituminous thicknesses obtained using the metal plate method

Table 7 shows the dielectric constants and velocity values obtained by the amplitude or metal plate method with the air-coupled system. As in the case of the coring method, these values were calibrated at each control point of the three different cells by considering static measurements. The dielectric constants were obtained from Equation (3) and, then, the velocities were derived using Equation (2).

The dielectric constants obtained resulted on the order of the values obtained with the ground-coupled system when using the coring method – see Table 5. The velocities obtained range from 0.120 m/ns to

0.137 m/ns with average values of 0.126 m/ns, 0.131 m/ns and 0.128 m/ns for Cells 2, 3 and 4, respectively.

TABLE 5 – VELOCITIES OF PROPAGATION OBTAINED FROM THE CORING METHOD, FOR THE GROUND-COUPLED SYSTEM.

Cell	Line	Control point	Coring Thickness [m]	Velocity [m/ns]		ε	
				1.0 GHz	2.3 GHz	1.0 GHz	2.3 GHz
2	3	3.1	0.112	0.121	0.124	6.1	5.9
		3.2	0.115	0.128	0.126	5.5	5.7
	4	4.1	0.116	0.123	0.123	5.9	5.9
		4.2	0.115	0.126	0.127	5.7	5.6
3	5	5.1	0.064	0.125	0.130	5.7	5.3
		5.2	0.055	0.129	0.129	5.4	5.4
	6	6.1	0.055	0.129	0.134	5.4	5.0
		6.2	0.053	0.137	0.134	4.8	5.0
4	7	7.1	0.133	0.136	0.133	4.9	5.1
		7.2	0.134	0.125	0.128	5.8	5.5
	8	8.1	0.135	0.137	0.137	4.8	4.8
		8.2	0.128	0.136	0.134	4.9	5.0

TABLE 6 – VELOCITIES OF PROPAGATION OBTAINED FROM THE CORING METHOD, FOR THE AIR-COUPLED SYSTEM.

Cell	Line	Control point	Coring Thickness [m]	Velocity [m/ns]		ε	
				1.0 GHz	1.8 GHz	1.0 GHz	1.8 GHz
2	3	3.1	0.112	0.115	0.118	6.8	6.5
		3.2	0.115	0.118	0.116	6.5	6.7
	4	4.1	0.116	0.112	0.119	7.2	6.4
		4.2	0.115	0.117	0.117	6.6	6.6
3	5	5.1	0.064	0.126	0.129	5.7	5.4
		5.2	0.055	0.115	0.130	6.8	5.3
	6	6.1	0.055	0.117	0.123	6.8	5.9
		6.2	0.053	0.118	0.129	6.5	5.4
4	7	7.1	0.133	0.112	0.123	7.2	5.9
		7.2	0.134	0.118	0.117	6.5	6.8
	8	8.1	0.135	0.124	0.129	5.8	5.4
		8.2	0.128	0.115	0.125	6.8	5.7

TABLE 7 – VELOCITIES OF PROPAGATION AND THICKNESSES OBTAINED BY THE
AMPLITUDE METHOD, FOR THE AIR-COUPLED SYSTEM.

Cell	Line	Control point	ε		Velocity (m/ns)		Thickness (m)	
			1.0 GHz	1.8 GHz	1.0 GHz	1.8 GHz	1.0 GHz	1.8 GHz
2	3	3.1	5.6	5.7	0.126	0.126	0.123	0.119
		3.2	5.6	5.9	0.127	0.124	0.124	0.123
	4	4.1	5.8	6.2	0.125	0.120	0.129	0.118
		4.2	5.4	5.4	0.130	0.129	0.128	0.127
3	5	5.1	5.4	5.2	0.129	0.131	0.065	0.065
		5.2	5.4	5.2	0.129	0.131	0.062	0.055
	6	6.1	5.2	5.1	0.132	0.133	0.062	0.059
		6.2	5.3	5.2	0.130	0.132	0.058	0.054
4	7	7.1	5.9	5.3	0.123	0.130	0.147	0.141
		7.2	5.8	5.4	0.124	0.129	0.141	0.148
	8	8.1	5.7	4.9	0.126	0.135	0.137	0.142
		8.2	5.9	4.8	0.123	0.137	0.137	0.140

Next, thicknesses were obtained from Equation (4). Table 8 presents the thicknesses obtained from the amplitude method. The thicknesses obtained by the amplitude method (T_{AM}) were compared to the actual thicknesses obtained from coring (ground truth). The error (%) was evaluated as the difference between both thicknesses obtained from each calibration method, at the same control point, and normalized to the coring measures (T_{COR}) (Equation (5)). A maximum error of 12.7% was obtained.

$$error\ (\%) = \frac{|T_{AM} - T_{COR}|}{T_{COR}} \cdot 100 \tag{5}$$

Figure 25 presents a comparison between the thicknesses obtained from both coring and amplitude methods for the GSSI air-coupled system with the 1.0 GHz antenna. The data represented are the ones acquired by using the dynamic mode. For the profile line obtained by the amplitude method, the velocity was calculated for each trace using Equations (3) and (4). On the other hand, for the coring method, the average velocities obtained in VII were assumed (0.117 m/ns, 0.124 m/ns and 0.12 m/ns for Cells 2, 3 and 4, respectively).

Although the maximum error in Table 8 was obtained – at this frequency – for Cell 3, we think that such difference could represent an isolated result because the complete profiles obtained from the two

TABLE 8 – THICKNESSES OBTAINED BY THE AMPLITUDE METHOD AND COMPARISON
WITH THE THICKNESSES OBTAINED BY CORING.

| Cell	Control point	Thickness (m)			Comparison "*amplitude vs coring*"			
		Amplitude method		Coring	Difference (m)		Error (%)	
		1.0 GHz	1.8 GHz		1.0 GHz	1.8 GHz	1.0 GHz	1.8 GHz
2	3.1	0.123	0.119	0.112	0.011	0.007	9.8	6.2
	3.2	0.124	0.123	0.115	0.009	0.008	7.8	6.9
	4.1	0.129	0.118	0.116	0.013	0.002	11.2	1.7
	4.2	0.128	0.127	0.115	0.013	0.012	11.3	10.4
3	5.1	0.065	0.065	0.064	0.001	0.001	1.5	1.5
	5.2	0.062	0.055	0.055	0.007	0.000	12.7	0.0
	6.1	0.062	0.059	0.055	0.007	0.004	12.7	7.3
	6.2	0.058	0.054	0.053	0.005	0.001	9.4	1.9
4	7.1	0.147	0.141	0.133	0.014	0.008	10.5	6.0
	7.2	0.141	0.148	0.134	0.007	0.014	5.2	10.4
	8.1	0.137	0.142	0.135	0.002	0.007	1.5	5.2
	8.2	0.137	0.140	0.128	0.009	0.012	7.0	9.4
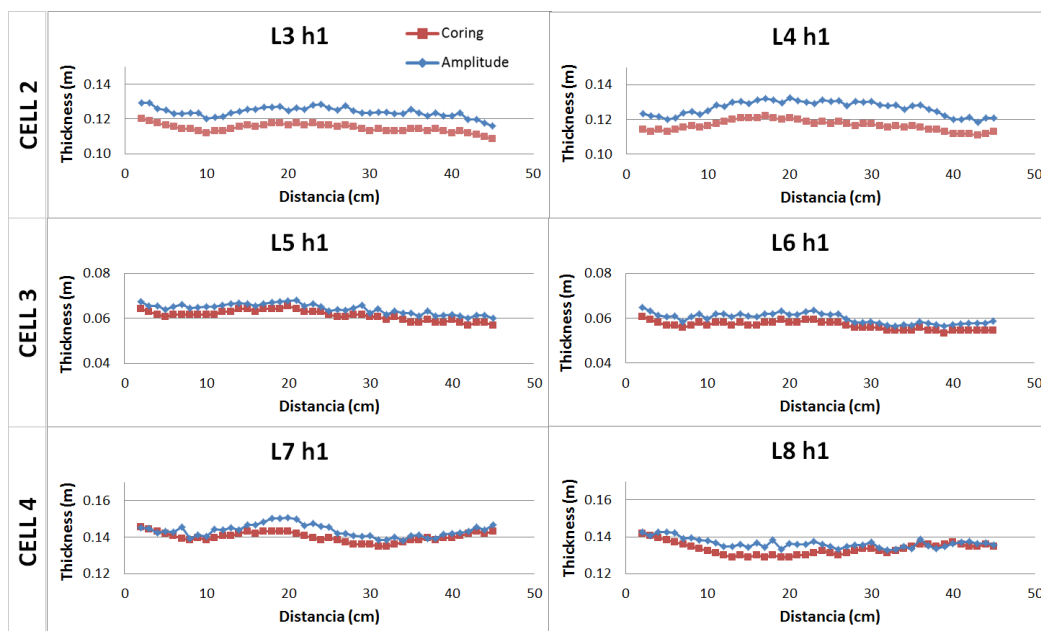
FIG. 25 – Comparison between the thicknesses obtained from both coring and
amplitude methods for the GSSI air-coupled system with the 1.0 GHz antenna.

methods show the best correlation. The maximum differences for thicknesses observed in Lines 3 and 4 are 11.0 mm and 14.0 mm, respectively. For Lines 5 and 6, the maximum differences are 3.0 mm and 4.0 mm, respectively, and for both Lines 7 and 8 the maximum differences are 8.0 mm.

4.3   TASK 3: EVALUATION OF THE FOULING LEVEL OF BALLAST.

Ballast fouling and moisture content are major issues in railway assessment usually leading to settlements of the railway. They can be easily evaluated by GPR as the dielectric value of the ballast increases with the presence of water [1]. This change is particularly relevant on contaminated ballast as the fine soil particles are more susceptible to the increase of water content of the material due to the decrease of drainage capabilities [7].

Some laboratory tests were developed during the STSM presented in this paper, to evaluate the dielectric constants for different levels of fouled ballast (0, 7.5% and 15%). The effect of water content on the dielectric constant was also evaluated, and different water contents were considered: 5.5%, 10% and 14%. For the evaluation, two different GPR systems, with air- and ground-coupled antennas working at different frequencies and manufactured by different companies, were used – same as in the previous sections.

Firstly, the influence of the ballast condition on the dielectric constant was analysed. Table 9 displays the results obtained. Significant differences were not observed between the dielectric constants obtained for new (Box 1) and used (Box 2) ballast, the used ballast gave slightly higher values compared to the new material.

Table 10 shows the results obtained when simulating a fouling ballast of 7.5%, as well as the influence of water content. Different levels of water content were simulated: 5.5%, 10% and 14% - as already mentioned. As expected, the comparison of fouling ballast 0% -Table 9, 7.5% - Table 10 and 15% - Table 11, with 5.5% of water content, has demonstrated that dielectric values increase with the increasing of fouling conditions.

The dielectric constant also increases with the water content. However, the analysis of all the values obtained has revealed that values are more sensitive to the fouling level rather than with the water content. Thus,

Open access | www.GPRadar.eu/journal
Volume 1 | Issue 1 | January 2018

100

Published in Rome, Italy
by TU1208 GPR Association

https://doi.org/10.26376/GPR2018004

the increasing of fouling reflected in a major dielectric constant variation. Different tendencies were found between the different equipment used, and the dielectric constants obtained with a frequency of 1.0 GHz were slightly lower than those obtained with higher frequencies of 1.8 GHz and 2.3 GHz. This behaviour was observed for both air- and ground-coupled antennas. Similar differences were found in [8] between the frequencies of 500 MHz and 900 MHz.

TABLE 9 – DIELECTRIC CONSTANTS OBTAINED FOR NEW (BOX 1) AND OLD (BOX 2) BALLAST WITH 0% FOULING AND 5.5% OF WATER CONTENT.

			Dielectric constant			
			Air-coupled		Ground-coupled	
Fouling (%)	Control point	Box	1.0 GHz	1.8 GHz	1.0 GHz	2.3 GHz
0	1.1	1	4.87	4.64	4.01	3.87
0	1.2	1	4.62	4.55	3.58	3.74
0	2.1	2	5.3	4.7	4.2	3.9
0	2.2	2	4.6	4.7	3.8	3.6

TABLE 10 – DIELECTRIC CONSTANTS OBTAINED FOR NEW BALLAST (BOX 3) SIMULATING 7.5% FOULING AND CONSIDERING DIFFERENT WATER CONTENTS OF 5.5, 10 AND 14%.

				Dielectric constant			
				Air-coupled		Ground-coupled	
Fouling (%)	Water (%)	Control point	Box	1.0 GHz	1.8 GHz	1.0 GHz	2.3 GHz
7.5	5.5	3.1	3	5.5	5.0	4.2	4.5
7.5	5.5	3.2	3	5.1	4.8	4.4	3.7
7.5	10	3.1	3	5.8	5.0	4.6	4.9
7.5	10	3.2	3	5.1	5.0	4.7	4.6
7.5	14	3.1	3	6.2	5.8	5.2	5.1
7.5	14	3.2	3	5.2	5.2	4.7	4.6

Open access | www.GPRadar.eu/journal
Volume 1 | Issue 1 | January 2018

101

Published in Rome, Italy
by TU1208 GPR Association

https://doi.org/10.26376/GPR2018004

TABLE 11 – Dielectric constants obtained for old ballast (box 4) simulating 15% fouling and considering different water contents of 5.5, 10 and 14%.

| | | | | Dielectric constant | | | |
| | | | | Air-coupled | | Ground-coupled | |
Fouling (%)	Water (%)	Control point	Box	1.0 GHz	1.8 GHz	1.0 GHz	2.3 GHz
15	5.5	4.1	4	6.5	5.9	5.4	4.6
15	5.5	4.2	4	6.0	5.5	5.3	4.3
15	10	4.1	4	6.9	6.5	5.8	5.1
15	10	4.2	4	6.7	6.1	5.9	4.9
15	14	4.1	4	7.1	7.2	6.1	5.7
15	14	4.2	4	7.1	6.8	5.9	5.1

Additionally, the dielectric constants obtained for the increasing fouling conditions and water content, with a central frequency of 1.0 GHz, were different for the two radar systems. The results obtained with the MALÅ system were slightly lower than those obtained with the GSSI system. Although a similar behaviour was observed in Task 2, when estimating asphalt thicknesses, the difference could be also caused by the limited size of the boxes (0.65 m long, 0.2 m high and 0.4 m wide). The transmitted signal could be affected by boundary effects, which are obviously much more significant when the antenna is suspended (air-coupled antennas).

CONCLUSIONS

In this work, we performed a series of experiments to study the Ground Penetrating Radar (GPR) detection of track defects at infrastructure level (voids and cracking) in railways, the measurement of layer thickness, and the evaluation of the fouling level of ballast. We used two different GPR systems, equipped with ground- and air-coupled antennas working at different frequencies. We also combined GPR results with Falling Weight Deflectometer and Light Falling Weight Deflectometer data.

ACKNOWLEDGEMENTS

Open access | www.GPRadar.eu/journal
Volume 1 | Issue 1 | January 2018

102

Published in Rome, Italy
by TU1208 GPR Association

https://doi.org/10.26376/GPR2018004

REFERENCES

[1]   T. R. Sussmann, K. R. Maser, D. Kutrubes, F. Heyns, and E. T. Selig, "Development of Ground Penetrating Radar for railway infrastructure condition detection," Proc. Symposium on the Application of Geophysics to Engineering and Environmental Problems, pp. RBA4–RBA4, 2001.

[2]   C. Esveld, Modern railway track, Zaltbommel, MRT-Productions, 2001.

[3]   E. Berggren, Railway track stiffness: dynamic measurements and evaluation for efficient maintenance, University West, 2009.

[4]   G. Manacorda, D. Morandi, A. Sarri, and G. Staccone, "Customized GPR system for railroad track verification," Proc. Ninth International Conference on Ground Penetrating Radar (GPR 2002), pp. 719–723, 2002.

[5]   S. Fontul, E. Fortunato, and F. De Chiara, "Non-Destructive Tests for Railway Infrastructure Stiffness Evaluation," B.H.V. Topping, Y. Tsompanakis, Stirlingshire, UK, 2011.

[6]   J. P. Hyslip, S. Chrismer, M. LaValley, and J. Wnek, "Track Quality From The Ground Up," Proc. AREMA Conference, Chicago, IL, 2012.

[7]   F. De Chiara, S. Fontul, and E. Fortunato, "GPR Laboratory Tests For Railways Materials Dielectric Properties Assessment," Remote Sensing 6(10), pp. 9712–9728, 2014.

[8]   E. Fortunato, "Renovação de Plataformas Ferroviárias. Estudos Relativos à Capacidade de Carga," Ph.D. Thesis (in Portuguese), Departamento de Engenharia Civil; Porto: Faculdade de Engenharia da Universidade do Porto, 2005.

Open access | www.GPRadar.eu/journal
Volume 1 | Issue 1 | January 2018

103

Published in Rome, Italy
by TU1208 GPR Association

https://doi.org/10.26376/GPR2018004